



High reversible capacity of SnO₂/graphene nanocomposite as an anode material for lithium-ion batteries

Peichao Lian^a, Xuefeng Zhu^b, Shuzhao Liang^a, Zhong Li^a, Weishen Yang^b, Haihui Wang^{a,*}

^a School of Chemistry & Chemical Engineering, South China University of Technology, No. 381 Wushan Road, Guangzhou 510640, China

^b State Key Laboratory of Catalysis, Dalian Institute of Chemical Physics, Chinese Academy of Sciences, Dalian 116023, China

ARTICLE INFO

Article history:

Received 11 December 2010

Received in revised form 19 January 2011

Accepted 31 January 2011

Available online 24 February 2011

Keywords:

Graphene sheets

SnO₂ nanoparticles

Nanocomposite

Anode material

Lithium-ion batteries

ABSTRACT

A gas–liquid interfacial synthesis approach has been developed to prepare SnO₂/graphene nanocomposite. The as-prepared nanocomposite was characterized by X-ray diffraction, field emission scanning electron microscopy, transmission electron microscopy, and Brunauer–Emmett–Teller measurements. Field emission scanning electron microscopy and transmission electron microscopy observation revealed the homogeneous distribution of SnO₂ nanoparticles (2–6 nm in size) on graphene matrix. The electrochemical performances were evaluated by using coin-type cells versus metallic lithium. The SnO₂/graphene nanocomposite prepared by the gas–liquid interface reaction exhibits a high reversible specific capacity of 1304 mAh g⁻¹ at a current density of 100 mA g⁻¹ and excellent rate capability, even at a high current density of 1000 mA g⁻¹, the reversible capacity was still as high as 748 mAh g⁻¹. The electrochemical test results show that the SnO₂/graphene nanocomposite prepared by the gas–liquid interfacial synthesis approach is a promising anode material for lithium-ion batteries.

© 2011 Elsevier Ltd. All rights reserved.

1. Introduction

Lithium-ion batteries are currently the dominant power source for portable electronic devices and viewed as the promising power source of electrical/hybrid vehicles. Graphite is the widely commercial anode material, but its theoretical specific capacity is only 372 mAh g⁻¹ (by forming intercalation compounds (LiC₆)), which cannot fulfill the increasing demand for high performance lithium-ion batteries [1]. SnO₂ is concerned as a promising anode material for lithium-ion batteries due to the following two reasons [2,3]. Firstly, based on an alloying mechanism, SnO₂ + 4Li⁺ + 4e⁻ → 2Li₂O + Sn and Sn + xLi⁺ + xe⁻ → Li_xSn (0 ≤ x ≤ 4.4), its maximal theoretical capacity is 782 mAh g⁻¹ [4,5], which is more than twice that of the already-commercialized graphite (372 mAh g⁻¹) [6–8]. Secondly, the potential of the SnO₂ anode is higher than that of graphite, which reduces the potential safety problems with metallic lithium deposition on the host anode during rapid charge [1,3]. However, its application in practical lithium-ion batteries is still hampered by the poor cycling performance arising from the severe aggregation and huge volume changes of SnO₂ particles during Li insertion/extraction process [6–27]. The large volume changes of SnO₂ particles during lithium ions insertion/extraction process

causes cracking and crumbling, which will result in electrical disconnection of active material with current collector and consequently limit the cycling capability of electrodes [6–8,17–20]. The agglomeration of primitive particles drastically reduces the total entrance/exit sites available for Li⁺ ions and creates even more severe mechanical stresses in the surface region of a particulate aggregate, leading to poor electrochemical performance [13,23,25]. In order to alleviate the volume changes and agglomeration, two common strategies have been pursued. One strategy is to design hollow or porous structure SnO₂ anode materials [6–8,13,15,20,27]. Another one is to prepare SnO₂/C composites by loading SnO₂ nanoparticles into a ductile carbon matrix [9–12,17,18,21,25,26]. The second strategy is very effective to improve the electrochemical performance of SnO₂ material. The carbon in SnO₂/C composites can not only buffer the volume changes of SnO₂ nanoparticles and prevent them from aggregating to large particles but also increase electronic conductivity of composites due to its good electronic conductivity [5,9,10,12,16,23,25], which favors high rate performance.

Graphene, a monolayer of graphite, exhibits a number of intriguing unique properties [28,29], such as superior electronic conductivity, high surface area (theoretical value 2620 m² g⁻¹), large surface-to-volume ratio, good mechanical properties. Therefore, graphene is an ideal carbon nanostructure which can be used to design high performance SnO₂/carbon nanocomposite electrodes. So far, there have been a few reports about the preparation of SnO₂/graphene nanocomposite [30–36]. For example, Paek

* Corresponding author. Tel.: +86 20 87110131; fax: +86 20 87110131.
E-mail address: hhwang@scut.edu.cn (H. Wang).

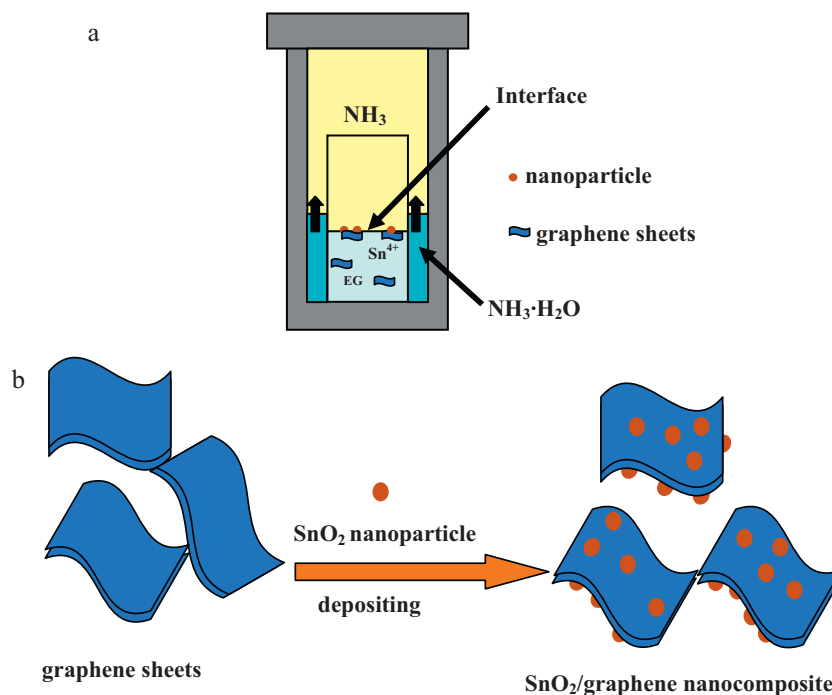


Fig. 1. (a) Schematic illustration for the reaction system and (b) synthesis process of SnO₂/graphene nanocomposite.

et al. [30] synthesized SnO₂/graphene nanocomposite with three-dimensionally delaminated flexible structure by mechanically mixing SnO₂ nanoparticles with graphene dispersions. The as-prepared SnO₂/graphene electrode material exhibited an enhanced cycle performance and lithium storage capacity. As claimed, the reversible capacity could remain 570 mAh g⁻¹ after 30 cycles that is about 70% retention of the original reversible capacity at a current density of 50 mA g⁻¹. Yao et al. [31] reported the in situ chemical synthesis of the SnO₂/graphene nanocomposite. The obtained SnO₂/graphene nanocomposite exhibits a reversible capacity of 765 mAh g⁻¹ in the first cycle and remains 520 mAh g⁻¹ after 100 cycles. Besides, some groups [32–35] prepared the SnO₂/graphene nanocomposite via in situ chemical synthesis route based on an oxidation–reduction reaction. The prepared SnO₂/graphene nanocomposite also shows enhanced electrochemical performance. However, the mechanically mixing method limits the homogeneous dispersion of SnO₂ nanoparticles and the separation of graphene sheets [31], and all those in situ chemical synthesis methods need extra thermal treatment, which makes the synthesis process complicated and time-consuming. Furthermore, these SnO₂/graphene nanocomposites only show relatively low reversible capacity. Therefore, it is still necessary to explore facile synthesis techniques for the preparation of SnO₂/graphene nanocomposite.

Recently, Cui et al. [37] prepared Fe₃O₄ nanoparticles by a facile gas–liquid interfacial reaction. Lian et al. [38] developed the gas–liquid interfacial synthesis approach and prepared Fe₃O₄/graphene nanocomposite. The Fe₃O₄/graphene nanocomposite prepared by the gas–liquid interfacial synthesis approach exhibited a very high reversible capacity. In this study, the facile gas–liquid interfacial synthesis approach was firstly used to prepare SnO₂/graphene nanocomposite. The as-prepared nanocomposite as an anode material for lithium-ion batteries exhibits an unprecedented high reversible specific capacity of 1304 mAh g⁻¹ after 150 cycles. Such excellent performance could be attributed to its porous structure and the enhanced surface electrochemical reactivity due to the large surface-to-volume ratio of SnO₂ nanoparticles [30].

2. Experimental

2.1. Materials preparation

All chemicals were of analytical grade and used as received, without further purification. Graphene sheets were prepared via a thermal exfoliation route involving graphite oxidation, following by rapid thermal expansion under nitrogen atmosphere. Detailed preparation procedure can be found in our previous paper [39]. SnO₂/graphene nanocomposite and SnO₂ nanoparticles were prepared by a gas–liquid interfacial reaction, as shown in Fig. 1. Briefly, in a 20-mL beaker, 0.3647 g of SnCl₄·5H₂O (Tianjin Kermel Chemical Reagent Co., Ltd., China) was dissolved in 10 mL of ethylene glycol (EG) (Beijing Chemical Reagent Co., Ltd., China), and then 0.0476 g of graphene sheets were added and sonicated for 6 h to yield a homogeneous suspension. Then the beaker was placed into a 100-mL Teflon-lined autoclave that contained 14 mL of ammonia solution (Guangzhou Chemical Reagent Factory, China). Then the autoclave was sealed and placed in a drying oven preheated to 180 °C and held at this temperature for 12 h. After cooling and centrifugation, washing with ethanol (Beijing Chemical Reagent Co., Ltd., China) for several times, the collected black solid product was dried at 100 °C in vacuum to obtain the desired SnO₂/graphene nanocomposite. The bare SnO₂ nanoparticles were synthesized under the same condition without the addition of graphene sheets for comparison.

2.2. Materials characterization

The structure and morphology of the as-prepared SnO₂/graphene nanocomposite and SnO₂ nanoparticles were characterized by X-ray diffraction (XRD, Bruker D8 Advance), scanning electron microscopy (SEM, Quanta 200F) and high-resolution transmission electron microscopy (HRTEM, FEI, Tecnai G² F30 S-Twin). N₂ adsorption/desorption isotherms were measured using a Micromeritics ASAP 2010 (USA) analyzer at liquid nitrogen temperature. Elemental analysis was carried out on vario EL III elemental (Germany) by burning the SnO₂/graphene nanocom-

posite to form carbon dioxide. The content of carbon (i.e., graphene sheets) in SnO₂/graphene nanocomposite was calculated according to the mass of carbon dioxide. The content of graphene in SnO₂/graphene nanocomposite was determined to be 22.76 wt.%. To reveal the reaction mechanism of SnO₂/graphene nanocomposite with Li, both of the fresh SnO₂/graphene electrode sheet and fully charged (3.0 V) one after 150 cycles were characterized by X-ray diffraction. The bare SnO₂ nanoparticles electrode sheets were also characterized for comparison.

2.3. Electrochemical measurement

The electrochemical measurements were carried out using the coin-type cells. The working electrode was prepared by mixing active material (SnO₂ nanoparticles or SnO₂/graphene nanocomposite) with poly(vinylidene fluoride) (PVdF, Kureha, Japan) and Super P carbon at a weight ratio of 75:10:15 in N-methyl-2-pyrrolidone (NMP, Tianjin Kermel Chemical Reagent Co., Ltd., China) to form a slurry. Then, the resultant slurry was uniformly pasted on Cu foil with a blade, dried at 120 °C in a vacuum oven (DZF-6020, Shanghai Qi Xin Scientific Instrument Co., Ltd., China) and pressed under a pressure of 20 MPa. The active material loading density of the electrode is ca. 1.0 mg cm⁻². The Celgard 2325 microporous membrane was used as separator. The electrolyte was 1 mol L⁻¹ LiPF₆ dissolved in a mixture of ethylene carbonate (EC) and dimethyl carbonate (DMC) (1:1 by volume) (Beijing Institute of Chemical Reagents, China). The lithium sheet was used as both counter and reference electrodes. CR2025-type coin cells were assembled in an argon-filled glove box and galvanostatically discharged and charged in a voltage range from 3.0 to 0.01 V using a Battery Testing System (Neware Electronic Co., China). Cyclic voltammetry (CV) measurements were carried out on an electrochemical workstation (Zahner IM6ex) over the potential range 0.01–3.0 V vs. Li/Li⁺ at a scanning rate of 0.2 mV s⁻¹.

3. Results and discussion

3.1. Microstructural characterization

As illustrated in Fig. 1, the beaker-in-autoclave setup is designed to confine the synthesis at the gas/liquid interface inside a sealed space [37,38]. SnCl₄ (Sn⁴⁺ species) and graphene sheets in EG solution were stored in the beaker, while aqueous ammonia solution (NH₃·H₂O) was placed in the autoclave liner outside the beaker. At room temperature, the beaker separates the two solutions. During the reaction, the system was heated to 180 °C quickly and then kept at that temperature for 12 h. Such a temperature increase results in the evaporation of ammonia, which reacts with Sn⁴⁺ at the gas/liquid interface to produce Sn(OH)₄ in situ deposited onto the graphene sheets [8,30]. The produced Sn(OH)₄ could be quickly decomposed to SnO₂ at 180 °C, and the SnO₂/graphene nanocomposite was formed in the beaker. Because all of the NH₃, Sn⁴⁺ and graphene sheets are homogeneously distributed at the gas/liquid interface, the formation of SnO₂/graphene nanocomposite is uniform and simultaneous at the interface. Furthermore, the reaction is limited at the interface, so that the particle growth is localized, which is important for synthesizing monodispersed nanoparticles with a narrow size distribution [37]. During the reaction, the convection inside the beaker will cause the graphene sheets to become immersed in the liquid and return back to the interface along the convection flow [37], which helps to achieve a homogeneous loading of SnO₂ nanoparticles on all the graphene sheets. It is very important to choose EG as the solvent in the beaker-in-autoclave setup. Firstly, EG is a good dispersant for graphene sheets, which

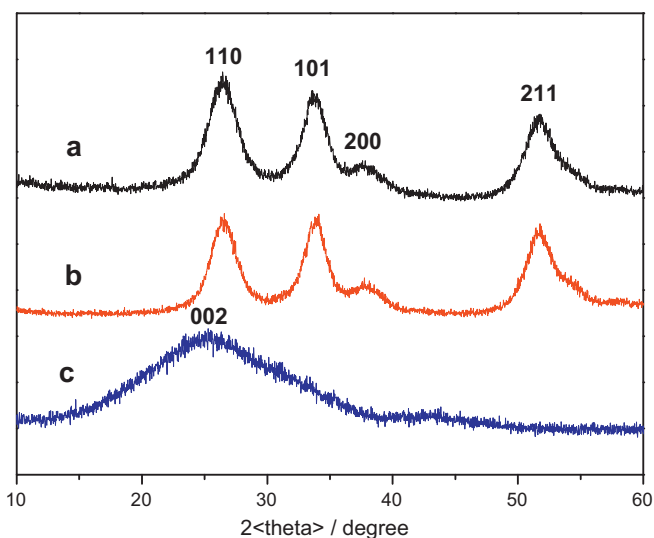


Fig. 2. XRD patterns of the as-synthesized (a) SnO₂/graphene nanocomposite and (b) SnO₂ nanoparticles, they are identified as tetragonal SnO₂ (JCPDS file card no. 72-1147). (c) XRD pattern of graphene sheets.

is necessary for forming a homogeneous suspension. Secondly, EG is not a good solvent for NH₃, the reaction between NH₃ and Sn⁴⁺ was limited at the gas/liquid interface [37].

Fig. 2a and b shows XRD patterns of as-prepared SnO₂/graphene nanocomposite, SnO₂ nanoparticles. The diffraction peaks of crystalline SnO₂ nanoparticles are clearly distinguishable. All strong diffraction peaks can be indexed to the standard tetragonal SnO₂ phase (JCPDS file card no. 72-1147), indicating crystalline SnO₂ nanoparticles could be formed by the gas/liquid interfacial reaction. All peaks in the XRD pattern of SnO₂ nanoparticles are also in good agreement with those reported in the literature [30,31]. The broad diffraction peaks of the bare SnO₂ and SnO₂/graphene nanocomposite suggest that the nanoparticles are very small in size. There is a weak (002) diffraction peak in the XRD pattern of graphene sheets as shown in Fig. 2c. This result indicates that graphene sheets stacked into multilayers, leading to loss of their high surface area and intrinsic chemical and physical properties [31,33,34]. However, no obvious diffraction peak attributed to graphite in the XRD pattern of SnO₂/graphene nanocomposite was observed. This result indicates that the SnO₂ nanoparticles deposited on graphene sheets can prevent them from stacking into multilayers, favoring the maintenance of high surface area and intrinsic chemical and physical properties of graphene sheets [31,33,34]. The average crystal size of SnO₂ nanoparticles in the SnO₂/graphene nanocomposite is around 3.7 nm calculated by Scherrer's formula based on the (110) peak.

The SEM and TEM micrographs of SnO₂ nanoparticles, graphene sheets and SnO₂/graphene nanocomposite are shown in Fig. 3. As shown in Fig. 3a and e, the SnO₂ nanoparticles prepared by the gas-liquid interfacial reaction aggregated into large particles. The resulting large particles could be easily pulverized owing to an asymmetrical volume change during Li⁺ insertion/extraction process, resulting in capacity decay as an anode material for lithium-ion batteries [13,23,25]. Fig. 3b presents the representative SEM image of graphene sheets from the top view, showing the layered platelets composed of curled nanosheets, which is accordant to the weak (002) diffraction peak in the XRD pattern of the bare graphene sheets. Fig. 3c shows the SEM image of SnO₂/graphene nanocomposite prepared by the facile gas-liquid interfacial synthesis approach. Obviously, the deposition of SnO₂ nanoparticles onto the surfaces of graphene sheets is homogeneous. The SnO₂ nanoparticles are uniformly distributed on 2D

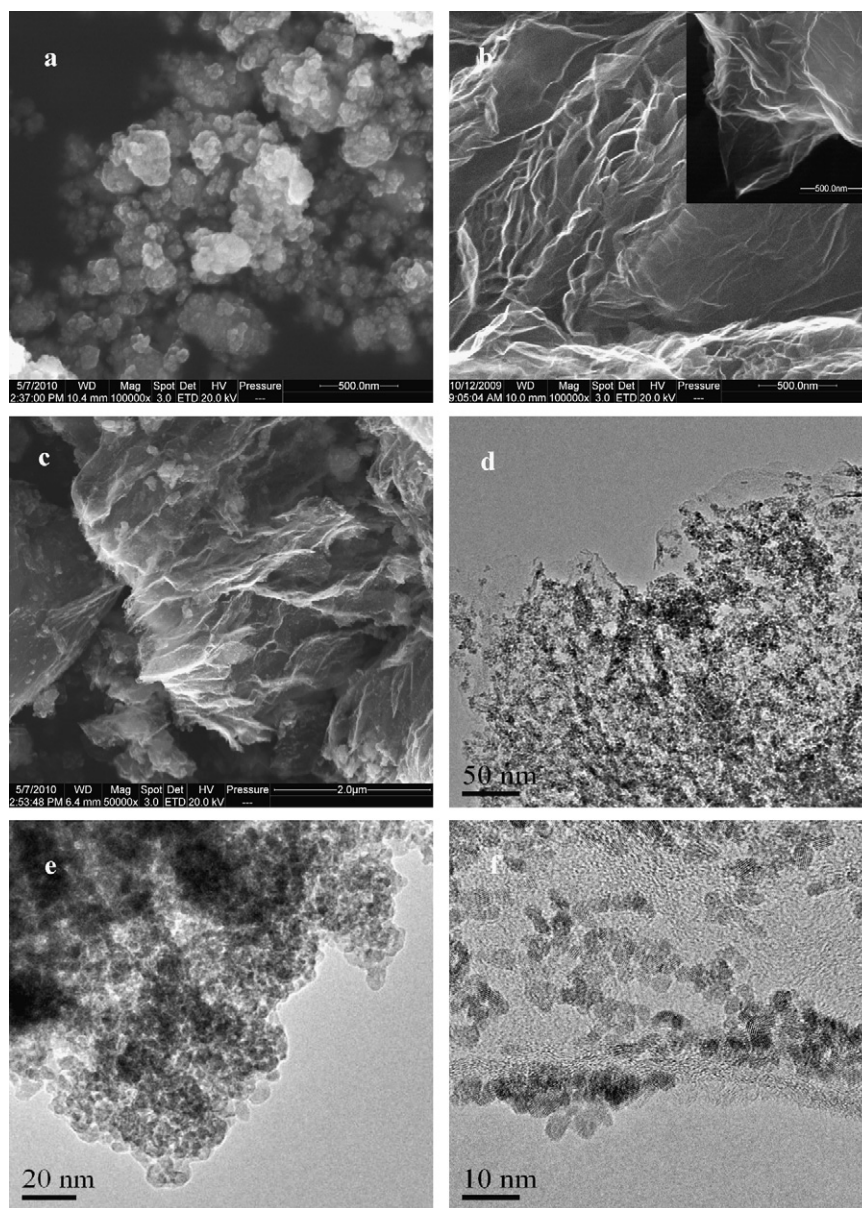


Fig. 3. SEM and TEM observation of SnO₂ nanoparticles, graphene sheets and SnO₂/graphene nanocomposite: SEM micrographs of (a) SnO₂ nanoparticles, (b) graphene sheets (inset shows the edge-side of graphene sheets) and (c) SnO₂/graphene nanocomposite. Low-magnification TEM images of (d) SnO₂/graphene nanocomposite. High-magnification TEM images of (e) SnO₂ nanoparticles, (f) SnO₂/graphene nanocomposite.

graphene sheets in as-prepared SnO₂/graphene nanocomposite, as shown in Fig. 3d. From Fig. 3c and d, it can be observed that the graphene sheets are distributed between the SnO₂ nanoparticles and the nanoporous composite with large amount of void spaces was formed [30]. Such porous nanocomposite can possess excellent cycle performance as an anode material for lithium-ion batteries due to the large amount of void spaces which could buffer large volume changes of SnO₂ nanoparticles during lithium ions insertion/extraction process [7,8,12,16,18,30,38]. Moreover, the graphene sheets distributed between the SnO₂ nanoparticles can prevent the aggregation of these nanoparticles to a certain extent [9,14,25,32,38], which can be of great benefit to cycle life. The nanoparticles deposited on graphene sheets can also prevent them from stacking into multilayers [31,33,34], matching well with the result that no obvious diffraction peak attributed to graphite in the XRD pattern of SnO₂/graphene nanocomposite was observed. It should be pointed out that the random hybridiza-

tion between SnO₂ nanoparticles and ultrathin graphene sheets can form highly conducting 3D graphene electronic conductive network and porous structure of the SnO₂/graphene nanocomposite [38]. The formed highly conducting 3D graphene electronic conductive network could increase electronic conductivity of the nanocomposite and the porous structure can facilitate liquid electrolyte diffusion into the bulk materials, which is beneficial for achieving high rate performance [7,8,30,31,34]. The HRTEM images (Fig. 3e and f) revealed that the average particle size of SnO₂ nanoparticles in the SnO₂/graphene nanocomposite is comparable to that of bare SnO₂ nanoparticles. Both of them are less than 6 nm. The average particle size of SnO₂ nanoparticles (ca. 4 nm) in the SnO₂/graphene nanocomposite observed from the HRTEM image is also well consistent with that estimated by the Scherrer equation. The small SnO₂ nanoparticles can provide short diffusion length for lithium ions insertion, resulting in good rate capability [7,38]. More importantly, even after a long time of sonication

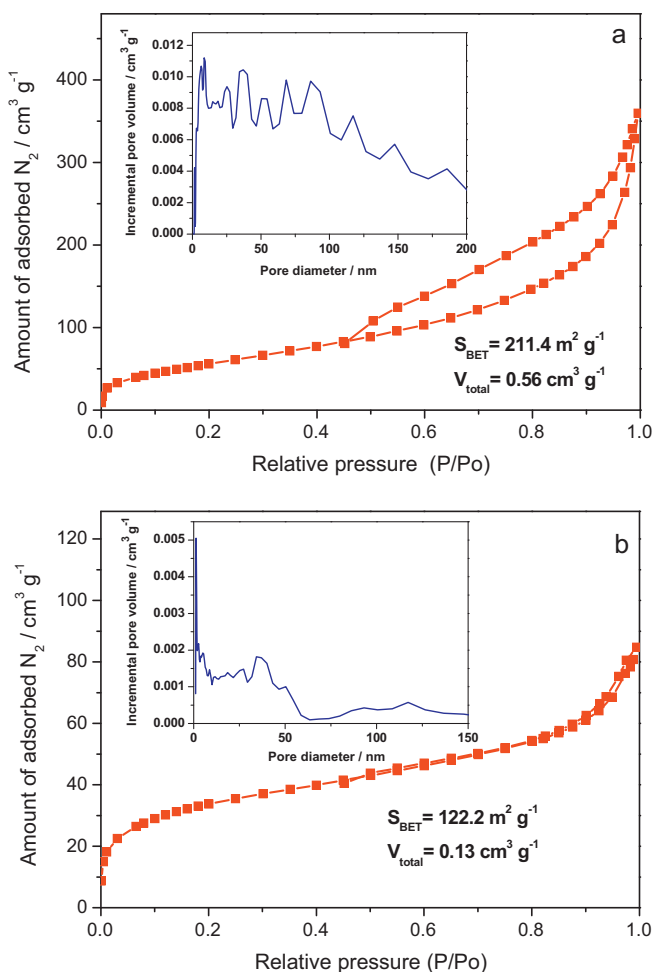


Fig. 4. Nitrogen adsorption/desorption isotherms of (a) SnO₂/graphene nanocomposite and (b) SnO₂ nanoparticles, insets show the pore-size distribution by original density functional theory model.

during the preparation of the TEM specimen, the SnO₂ nanoparticles were still strongly anchored on the surface of graphene sheets with a high density (shown in Fig. 3d and f), implying the strong interaction between SnO₂ nanoparticles and graphene sheets [38].

N₂ adsorption/desorption isotherms were employed to investigate the pore structures of SnO₂/graphene nanocomposite and the bare SnO₂ nanoparticles, as shown in Fig. 4. The Brunauer–Emmett–Teller (BET) specific surface area of SnO₂/graphene and SnO₂ nanoparticles are about 211.4 and 122.2 m² g⁻¹, respectively. Obviously, the BET specific surface area of SnO₂/graphene nanocomposite is higher than that of SnO₂ nanoparticles, which could lead to its increased electrochemical reactive activity [30,40,41]. The SnO₂/graphene nanocomposite possesses a much better porosity than bare SnO₂ nanoparticles. The total pore volume of SnO₂/graphene nanocomposite (0.56 cm³ g⁻¹) is much larger than that of the SnO₂ nanoparticles (0.13 cm³ g⁻¹). The increased pore volume could arise primarily from the formation of secondary pores between the SnO₂ nanoparticles and graphene sheets as well as the close stacking of graphene sheets distributed between the SnO₂ nanoparticles [38]. The nanopores in SnO₂/graphene nanocomposite could act as buffering spaces against the volume changes of SnO₂ nanoparticles during lithium ion insertion/extraction process [7,8,13,14,18,38], which would lead to enhanced cycling stability as an anode material for lithium-ion batteries.

3.2. Electrochemical properties of SnO₂/graphene nanocomposite and SnO₂ nanoparticles

The electrochemical properties of the SnO₂/graphene nanocomposite and the bare SnO₂ nanoparticles were investigated using coin-type cells. The first 100 discharge/charge cycles were tested at a current density of 100 mA g⁻¹, and the corresponding discharge/charge curves are shown in Fig. 5a. The initial small plateaus and long slope profiles of SnO₂/graphene nanocomposite is similar to that of bare SnO₂ nanoparticles. Their first discharge voltage profiles both show classic plateaus in the potential ranging from 0.8 to 1.5 V, which was mainly due to the conversion reaction between SnO₂ and Li, $\text{SnO}_2 + 4\text{Li}^+ + 4e^- \rightarrow 2\text{Li}_2\text{O} + \text{Sn}$, leading to in situ formation of Sn–Li₂O nanocomposites [13,33,41,42].

As shown in Fig. 5b, the initial reversible specific capacity of the SnO₂ nanoparticles is 603.4 mA h g⁻¹. After the first cycle, the charge specific capacity increases to 639.9 mA h g⁻¹ in the 3rd cycle, indicating an activation process in the material [9]. The activation process is due to the aggregation of SnO₂ nanoparticles, which result in that only part of active material is involved in the initial reaction. During the first Li insertion/extraction process, the aggregated SnO₂ particles were pulverized into small particles due to their large volume changes [13,30,31], resulting in more active materials are involved in the 2nd and 3rd cycles. However, the pulverization of in situ formed Sn particles during the first three cycles destroyed the electronic conducting network between the active material and current collector [5,7,33], resulting in the reversible capacity decay from the 4th cycle. The reversible capacity of bare SnO₂ nanoparticles remains only 198.2 mA h g⁻¹ after 100 cycles. As shown in Fig. 3c and d, SnO₂ nanoparticles are tightly attached to the graphene sheets and spatially separated by the graphene sheets in the SnO₂/graphene nanocomposite, which are favorable for improving the cycling performance [9,31,33]. In addition, the nanosized SnO₂ particles and the elastic graphene sheets in the porous SnO₂/graphene nanocomposite also help to accommodate the volume changes and prevent the pulverization of SnO₂ to a certain extent during discharge/charge cycles [13,30–34], which would lead to excellent cycle capability. As shown in Fig. 5b, the SnO₂/graphene nanocomposite indeed shows enhanced electrochemical performances as expected. The charge capacity of the nanocomposite is as high as 936.4 mA h g⁻¹ in the first cycle and decreases to 732.2 mA h g⁻¹ in the 20th cycle. Nevertheless, the reversible capacity begins increasing from 21st cycle and increases to 1156.4 mA h g⁻¹ in the 100th cycle. The phenomenon, the reversible specific capacity decreases to a low value then gradually increases, has never been reported for SnO₂/C composites. But the similar phenomenon has been reported for Fe₃O₄/C composites [43]. The decay of reversible capacity of the SnO₂/graphene during the first 20 cycles could be due to the pulverization of original SnO₂ and in situ formed Sn nanoparticles during Li insertion/extraction process, which lead to loss of electrical connectivity between neighboring particles [17]. During discharge/charge cycles, the in situ formed Sn nanoparticles became smaller and smaller due to electrochemical milling effect [44] and attached on the graphene sheets tightly. It is reported that activation energies for solid-state double decomposition reactions decreased with decreasing reagent particle size [45]. Thus, the conversion reaction, $\text{SnO}_2 + 4\text{Li}^+ + 4e^- \rightarrow 2\text{Li}_2\text{O} + \text{Sn}$, which is usually reported to be irreversible [9,41], can become reversible in the SnO₂/graphene nanocomposite due to the very small Sn nanoparticles [5,27,46–49]. It has been reported that the Sn–Li alloying and dealloying reactions only occur below 1.0 V (vs. (Li/Li⁺)) [4,10,50] and the Li–O bonds are not stable when the charge potential is above 1.3 V [50]. As shown in Fig. 5a, there is a plateau at around 1.3 V at the charge curves of SnO₂/graphene nanocomposite, indicating the reaction $\text{SnO}_2 + 4\text{Li}^+ + 4e^- \rightarrow 2\text{Li}_2\text{O} + \text{Sn}$ indeed

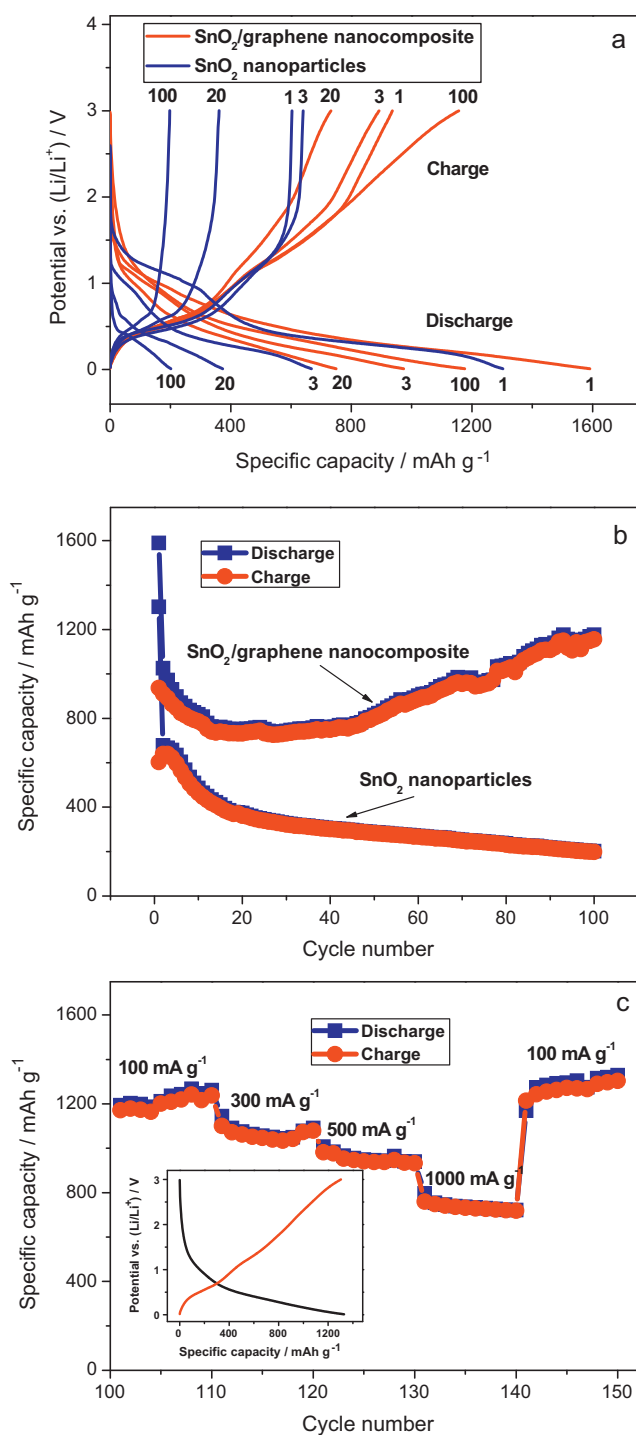


Fig. 5. (a) Discharge/charge profiles of SnO₂/graphene nanocomposite and SnO₂ nanoparticles at a current density of 100 mA g⁻¹. (b) Capacities versus cycle number between 3 V and 0.01 V at the current density of 100 mA g⁻¹. (c) Cycling performance of SnO₂/graphene nanocomposite at various current densities (the same cell after cycled for 100 cycles shown in b), inset shows the 150th discharge/charge voltage profiles.

became partially reversible in the SnO₂/graphene nanocomposite. The plateau above 1.0 V in the 100th charge curve is longer than that at the 20th charge curve, suggesting that the electrochemical reactivity increased due to the reduced Sn and Li₂O nanoparticles with increasing cycle number. It is very possible that the increasing electrochemical reactivity results in the increase of reversible capacity of SnO₂/graphene nanocomposite after 20 cycles. It should

be pointed out that although a plateau above 1.0 V was observed in both the first and third charge curves of bare SnO₂ nanoparticles, it completely disappeared in the 20th cycle. This result indicates that the reaction between bare SnO₂ nanoparticles and Li, $\text{SnO}_2 + 4\text{Li}^+ + 4\text{e}^- \rightarrow 2\text{Li}_2\text{O} + \text{Sn}$, is partially reversible during the first several cycles, but the reversibility decrease with increasing cycle number due to the decreasing electrochemical reactivity because of the aggregation of in situ formed Sn nanoparticles [5,13,24,25]. In contrast, a charge plateau above 1.0 V constantly existed during all the charge/discharge cycles of the SnO₂/graphene nanocomposite, indicating that the reaction between SnO₂ and Li, $\text{SnO}_2 + 4\text{Li}^+ + 4\text{e}^- \rightarrow 2\text{Li}_2\text{O} + \text{Sn}$, is constantly reversible. The possible reason is that the graphene sheets in the SnO₂/graphene nanocomposite can prevent the aggregation of in situ formed Sn nanoparticles [10,22]. The initial coulombic efficiency of the SnO₂/graphene is 59%, but it is above 94% after 5 cycles. The large irreversible capacity during the first cycle can be attributed to irreversible lithium loss due to the formation of thick solid-electrolyte interface (SEI) layer on the electrode surface [5,17,35], and the fact that some Sn(0) cannot be re-oxidized back to Sn(IV) [9,19]. Table 1 shows a comparison of the reversible specific capacity at a low current density between the SnO₂/graphene nanocomposites reported before and in this work. Obviously, the SnO₂/graphene nanocomposite prepared by the facile gas-liquid interfacial synthesis approach possesses higher reversible specific capacity and better cycle performance than those reported previously.

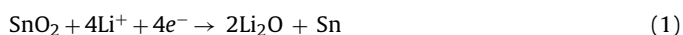
After 100 cycles, the same cell was further evaluated for rate capability as shown in Fig. 5c. When the same cell was tested at various current densities from 100 to 1000 mA g⁻¹, the SnO₂/graphene nanocomposite exhibits an excellent rate capability. At the high current densities of 300, 500 and 1000 mA g⁻¹, the SnO₂/graphene nanocomposite can still exhibit high reversible capacities of 1072, 976 and 748 mAh g⁻¹, respectively. All of these values are more than twice the theoretical specific capacity of the commonly used graphite anode material (372 mAh g⁻¹). Such excellent rate capability should be attributed to the highly conducting 3D graphene electronic conductive network and porous structure of the SnO₂/graphene nanocomposite. The highly conducting 3D graphene electronic conductive network could increase electronic conductivity of the nanocomposite and the porous structure can facilitate liquid electrolyte diffusion into the bulk materials [7,30,34,35,41]. In addition, the shorten path length for Li⁺ transport due to nanosized SnO₂ particles in as-prepared SnO₂/graphene nanocomposite can also favor the high rate capability [7,41]. Remarkably, when the current density returns to the initial 100 mA g⁻¹ after more than 140 cycles, a high reversible specific capacity of 1304 mAh g⁻¹ can be obtained in the 150th cycle. The reversible capacity of 1304 mAh g⁻¹ is much higher than the theoretical specific capacity of the SnO₂/graphene nanocomposite (858 mAh g⁻¹) calculated according to the theoretical specific capacity of SnO₂ (782 mAh g⁻¹ based on the conventional alloying mechanism) and graphene sheets (1116 mAh g⁻¹) [38,39]. This result gives assistant information that the conversion reaction of SnO₂ in the SnO₂/graphene nanocomposite, $\text{SnO}_2 + 4\text{Li}^+ + 4\text{e}^- \rightarrow 2\text{Li}_2\text{O} + \text{Sn}$, should be reversible to a certain extent. Such a result can be related to the enhanced surface electrochemical reactivity due to its large BET specific surface area and nanocrystalline nature [30,40,41,48]. Based on the novel conversion and alloying mechanism, $\text{SnO}_2 + 4\text{Li}^+ + 4\text{e}^- \rightleftharpoons 2\text{Li}_2\text{O} + \text{Sn}$ and $\text{Sn} + x\text{Li}^+ + xe^- \rightleftharpoons \text{Li}_x\text{Sn}$ ($0 \leq x \leq 4.4$) [25], the maximum theoretical specific capacity of SnO₂ is 1493 mAh g⁻¹, and the theoretical specific capacity of SnO₂/graphene nanocomposite should be as high as 1407 mAh g⁻¹. This theoretical value is quite close to the experimental one of 1304 mAh g⁻¹.

The cyclic voltammetry of the as-prepared SnO₂/graphene nanocomposite is shown in Fig. 6a. In the cathodic polarization pro-

Table 1
Reversible specific capacities of SnO₂/graphene nanocomposites reported before and in this work.

Current density/mA g ⁻¹	Initial capacity/mAh g ⁻¹	Cycle number	Remaining capacity/mAh g ⁻¹	Ref.
50	810	30	570	[30]
55	765	100	520	[31]
67	978	30	840	[32]
264	786	50	558	[33]
50	862	50	665	[34]
200	541	35	377	[35]
100	936	100	1156	This work

cess of the first cycle, two obvious peaks were observed at 0.90 and 0.03 V. The peak at 0.90 V could be ascribed to the formation of solid electrolyte interface (SEI) layer on the surface of active material [9,31,40], reduction of SnO₂ to Sn and the synchronous formation of Li₂O [32,48] as described in Eq. (1):



The peak at 0.90 V is in good agreement with the first discharge voltage plateau during the discharge/charge tests. The peak at 0.03 V corresponds to alloying of Sn with Li and the reversible reaction between lithium and graphene sheets [17,31,32,38,39], as described in Eqs. (2) and (3) respectively:

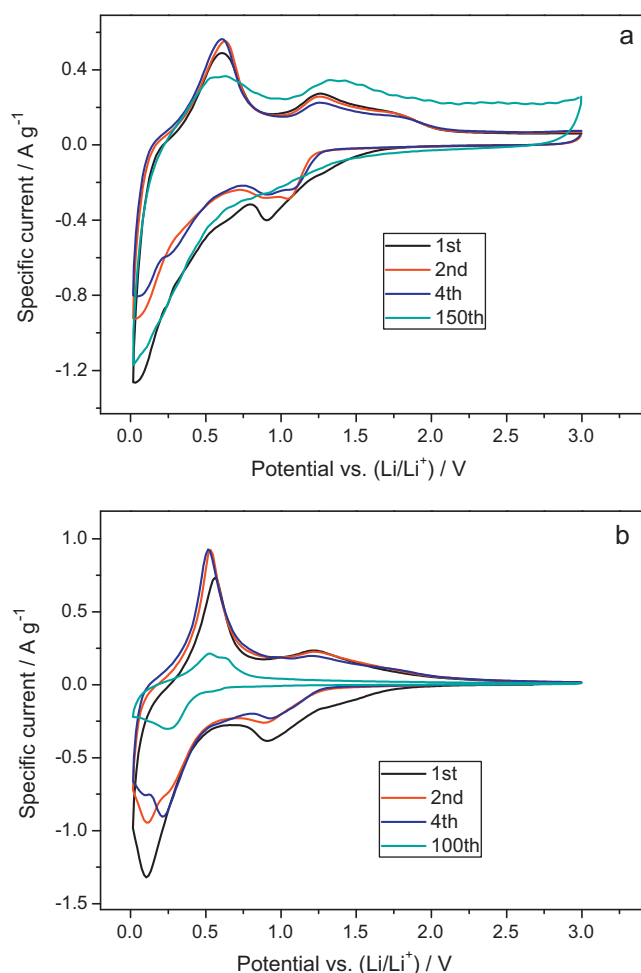
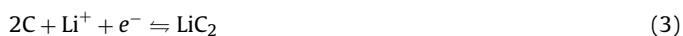
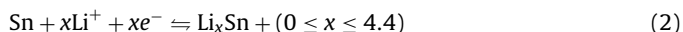
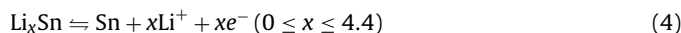


Fig. 6. Cyclic voltammograms (CV) of (a) SnO₂/graphene nanocomposite and (b) SnO₂ nanoparticles at a scanning rate of 0.2 mV s⁻¹.

Meanwhile, in the anodic polarization process, two peaks were recorded at about 0.60 and 1.26 V. The peak at 0.60 V represents the de-alloying process of Li⁺ ions [48] as described in Eq. (4):



The following peak at 1.26 V could be ascribed to in part reversible reaction of the Eq. (1) [31]. After the first cycle, the peak intensity of CV curve in the 4th cycle becomes lower than that in the 2nd cycle. However, the peak intensity of the CV curve in the 150th is still very high, and the integral area is also very big, revealing the good cycling stability. Note that a peak at 1.32 V at the 150th CV curve of SnO₂/graphene nanocomposite is observed, which indicates that the Eq. (1) is at least partially reversible in the SnO₂/graphene nanocomposite [5,17,27]. This result is in good agreement with that of galvanostatically discharged and charged tests. For the bare SnO₂ nanoparticles in Fig. 6b, there are still characteristic peaks at 0.91 and 0.10 V, corresponding to SEI layer formation and the alloying process, which also correspond to the reaction of lithium with SnO₂ during the first discharge process [5,9]. Although the CV curves of the bare SnO₂ nanoparticles in the 4th and 2nd cycles almost overlap, the peak intensity and integral area of the CV curve in the 100th cycle are obviously decreased, implying poor capacity retention. This result matches well with that of the discharge/charge tests.

To further confirm that the conversion reaction of SnO₂ in the SnO₂/graphene nanocomposite is partially reversible, the XRD patterns of electrode sheets before and after being cycled are shown in Fig. 7. As shown in Fig. 7c, the diffraction peaks of fully charged bare SnO₂ nanoparticles electrode sheets after 100

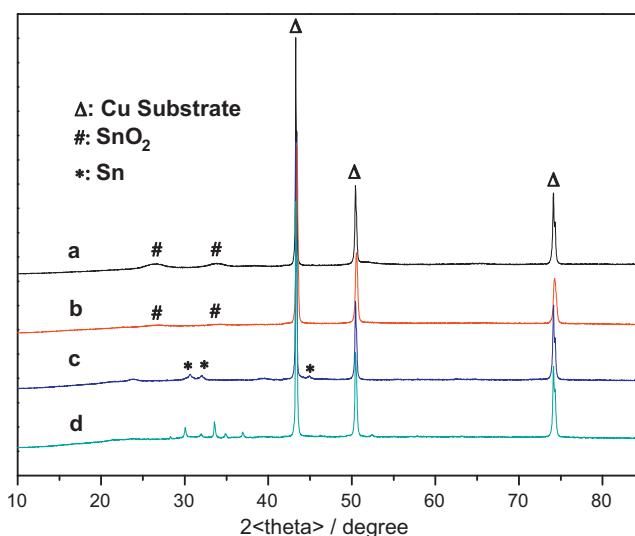


Fig. 7. XRD patterns of electrode sheets for (a) SnO₂ nanoparticles before being cycled, (b) SnO₂/graphene nanocomposite before being cycled, (c) SnO₂ nanoparticles after 100 cycles, and (d) SnO₂/graphene nanocomposite after 150 cycles.

cycles match well with characteristic peaks of Sn (JCPDS file card no. 04-0673), indicating that reaction mechanism of bare SnO₂ nanoparticles with Li is the usually reported alloying mechanism. In comparison, a diffraction peak at around 30.05° ascribed to SnO₂ (JCPDS file card no. 29-1484) is observed in the XRD pattern of fully charged SnO₂/graphene nanocomposite electrode sheet after 150 cycles, suggesting that the reaction mechanism of SnO₂ in the SnO₂/graphene nanocomposite is different from that of bare SnO₂ nanoparticles. This result is in good agreement with that of discharge/charge tests. The diffraction peaks of re-formed SnO₂ in the fully charged SnO₂/graphene nanocomposite electrode sheet are different from those of SnO₂ in the initial SnO₂/graphene nanocomposite electrode sheet, indicating that the structure of re-formed SnO₂ during cycles is different from that of initial SnO₂ [5]. The diffraction peak at around 34.85° was indexed to Sn (JCPDS file card no. 18-1380). The diffraction peak at around 33.54° matches well with characteristic peaks of Li₂O (JCPDS file card no. 12-0254). However, the crystal structures of Sn and Li₂O in the fully charged SnO₂/graphene nanocomposite electrode sheet are different from those in fully charged bare SnO₂ nanoparticles electrode sheets. The possible reason is that the graphene sheets in SnO₂/graphene nanocomposite can affect the crystal structures of formed Sn and Li₂O during cycles. The diffraction peaks at around 28.26°, 31.96° and 36.93° may be ascribed to the formed solid-electrolyte interface (SEI) layer on the electrode surface. The XRD results give extra evidence that the conversion reaction of SnO₂ in the SnO₂/graphene nanocomposite, $\text{SnO}_2 + 4\text{Li}^+ + 4\text{e}^- \rightarrow 2\text{Li}_2\text{O} + \text{Sn}$, is partially reversible.

4. Conclusions

In summary, SnO₂/graphene nanocomposite was prepared via a facile gas–liquid interfacial synthesis approach successfully. The preparation approach of SnO₂/graphene nanocomposite reported here is facile and inexpensive. We believe that the synthesis technique is promising for scaling up and technical implementation. The as-prepared SnO₂/graphene nanocomposite exhibits an unprecedented high reversible specific capacity of 1304 mAh g⁻¹ in the 150th cycle. This nanocomposite also exhibits excellent rate capability. Even at a high current density of 1000 mA g⁻¹, the reversible capacity is still as high as 748 mAh g⁻¹, more than twice the theoretic reversible capacity of graphite. The excellent electrochemical performances can be attributed to the following reasons: (1) the conversion reaction of SnO₂ in the SnO₂/graphene nanocomposite, $\text{SnO}_2 + 4\text{Li}^+ + 4\text{e}^- \rightarrow 2\text{Li}_2\text{O} + \text{Sn}$, becomes partially reversible during cycling due to enhancing surface electrochemical reactivity caused by its large BET specific surface area and nanocrystalline nature, which lead to its unprecedented high reversible specific capacity. (2) graphene sheets distributed between the SnO₂ nanoparticles can prevent their direct contact and thereby minimizing the aggregation of the SnO₂ nanoparticles during discharge/charge cycling process, resulting in high capacity retention. (3) the porous structure of SnO₂/graphene nanocomposite provides buffering spaces against the volume changes of SnO₂ nanoparticles during Li insertion/extraction process, leading to enhanced cycle performance. (4) the 3D graphene electronic conductive network, nanosized SnO₂ particles and porous structure of the SnO₂/graphene nanocomposite facilitate electron and lithium ion transport, favoring the high rate capability.

Acknowledgements

This work was financially supported by the National Natural Science Foundation of China (no. 20936001) and the Fundamental Research Funds for the Central Universities, SCUT (2009220038).

References

- [1] J.M. Tarascon, M. Armand, *Nature* 414 (2001) 359.
- [2] Y. Idota, T. Kubota, A. Matsufuji, Y. Maekawa, T. Miyasaka, *Science* 276 (1997) 1395.
- [3] M. Winter, J.O. Besenhard, *Electrochim. Acta* 45 (2006) 31.
- [4] I. Courtney, J.R. Dahn, *J. Electrochem. Soc.* 144 (1997) 2045.
- [5] M. Gao, X. Chen, H. Pan, L. Xiang, F. Wu, Y. Liu, *Electrochim. Acta* 55 (2010) 9067.
- [6] C. Wang, Y. Zhou, M. Ge, X. Xu, Z. Zhang, J.Z. Jiang, *J. Am. Chem. Soc.* 132 (2010) 46.
- [7] L. Li, X. Yin, S. Liu, Y. Wang, L. Chen, T. Wang, *Electrochem. Commun.* 12 (2010) 1383.
- [8] X. Yin, L. Chen, C. Li, Q. Hao, S. Liu, Q. Li, E. Zhang, T. Wang, *Electrochim. Acta* 56 (2011) 2358.
- [9] L. Noerochima, J.Z. Wang, S.L. Chou, H.J. Li, H.K. Liu, *Electrochim. Acta* 56 (2010) 314.
- [10] B. Liu, Z.P. Guo, G. Du, Y. Nuli, M.F. Hassanb, D. Jia, *J. Power Sources* 195 (2010) 5382.
- [11] S.L. Chou, J.Z. Wang, C. Zhong, M.M. Rahmana, H.K. Liu, S.X. Dou, *Electrochim. Acta* 54 (2009) 7519.
- [12] S. Yang, H. Song, H. Yi, W. Liu, H. Zhang, X. Chen, *Electrochim. Acta* 55 (2009) 521.
- [13] Y. Wang, J.Y. Lee, H.C. Zeng, *Chem. Mater.* 17 (2005) 3899.
- [14] Y. Wang, H.C. Zeng, J.Y. Lee, *Adv. Mater.* 18 (2006) 645.
- [15] D. Deng, J.Y. Lee, *Chem. Mater.* 20 (2008) 1841.
- [16] X.W. Lou, D. Deng, J.Y. Lee, L.A. Archer, *Chem. Mater.* 20 (2008) 6562.
- [17] X.W. Lou, J.S. Chen, P. Chen, L.A. Archer, *Chem. Mater.* 21 (2009) 2868.
- [18] X.W. Lou, C.M. Li, L.A. Archer, *Adv. Mater.* 21 (2009) 2536.
- [19] Y. Yu, C.H. Chen, Y. Shi, *Adv. Mater.* 19 (2007) 993.
- [20] Y. Yu, L. Gu, A. Dhanabalan, C.H. Chen, C. Wang, *Electrochim. Acta* 54 (2009) 7227.
- [21] R. Yang, W. Zhao, J. Zheng, X. Zhang, X. Li, *J. Phys. Chem. C* 114 (2010) 20272.
- [22] Y.S. Lin, J.G. Duh, M.H. Hung, *J. Phys. Chem. C* 114 (2010) 13136.
- [23] J. Liu, W. Li, A. Manthiram, *Chem. Commun.* 46 (2010) 1437.
- [24] P. Meduri, C. Pendyala, V. Kumar, G.U. Sumanasekera, M.K. Sunkara, *Nano Lett.* 9 (2009) 612.
- [25] H. Liu, D. Long, X. Liu, W. Qiao, L. Zhan, L. Ling, *Electrochim. Acta* 54 (2009) 5782.
- [26] J. Fan, T. Wang, C. Yu, B. Tu, Z. Jiang, D. Zhao, *Adv. Mater.* 16 (2004) 1432.
- [27] R. Demir-Cakan, Y.S. Hu, M. Antonietti, J. Maier, M.M. Titirici, *Chem. Mater.* 20 (2008) 1227.
- [28] A.K. Geim, K.S. Novoselov, *Nat. Mater.* 6 (2007) 183.
- [29] A.K. Geim, *Nature* 324 (2009) 1530.
- [30] S.M. Paek, E. Yoo, I. Honma, *Nano Lett.* 9 (2009) 72.
- [31] J. Yao, X. Shen, B. Wang, H. Liu, G. Wang, *Electrochem. Commun.* 11 (2009) 1849.
- [32] X. Wang, X. Zhou, K. Yao, J. Zhang, Z. Liu, *Carbon* 49 (2011) 133.
- [33] L.S. Zhang, L.Y. Jiang, H.J. Yan, W.D. Wang, W. Wang, W.G. Song, Y.G. Guo, L.J. Wan, *J. Mater. Chem.* 20 (2010) 5462.
- [34] Z. Du, X. Yin, M. Zhang, Q. Hao, Y. Wang, T. Wang, *Mater. Lett.* 64 (2010) 2076.
- [35] Y. Li, X. Lv, J. Lu, J. Li, *J. Phys. Chem. C* 114 (2010) 21770.
- [36] Z. Wang, H. Zhang, N. Li, Z. Shi, Z. Gu, G. Cao, *Nano Res.* 3 (2010) 748.
- [37] Z.M. Cui, L.Y. Jiang, W.G. Song, Y.G. Guo, *Chem. Mater.* 21 (2009) 1162.
- [38] P. Lian, X. Zhu, H. Xiang, Z. Li, W. Yang, H. Wang, *Electrochim. Acta* 56 (2010) 834.
- [39] P. Lian, X. Zhu, S. Liang, Z. Li, W. Yang, H. Wang, *Electrochim. Acta* 55 (2010) 3909.
- [40] M.S. Park, G.X. Wang, Y.M. Kang, D. Wexler, S.X. Dou, H.K. Liu, *Angew. Chem. Int. Ed.* 46 (2007) 750.
- [41] Y.J. Chen, C.L. Zhu, X.Y. Xue, X.L. Shi, M.S. Cao, *Appl. Phys. Lett.* 92 (2008) 223101.
- [42] Z. Ying, Q. Wan, H. Cao, Z.T. Song, S.L. Feng, *Appl. Phys. Lett.* 87 (2005) 113108.
- [43] L. Wang, Y. Yu, P.C. Chen, D.W. Zhang, C.H. Chen, *J. Power Sources* 183 (2008) 717.
- [44] Y. Yu, Y. Shi, C.H. Chen, C. Wang, *J. Phys. Chem. C* 112 (2008) 4176.
- [45] P.L. Taberna, S. Mitra, P. Poizot, P. Simon, J.M. Tarascon, *Nat. Mater.* 5 (2006) 567.
- [46] X. Sun, J. Liu, Y. Li, *Chem. Mater.* 18 (2006) 3486.
- [47] I. Sandua, T. Brousse, D.M. Schleich, M. Danot, *J. Solid State Chem.* 179 (2006) 476.
- [48] M. Xu, M. Zhao, F. Wang, W. Guan, S. Yang, X. Song, *Mater. Lett.* 64 (2010) 921.
- [49] S. Han, B. Jang, T. Kim, S.M. Oh, T. Hyeon, *Adv. Funct. Mater.* 15 (2005) 1845.
- [50] I.A. Courtney, J.R. Dahn, *J. Electrochem. Soc.* 144 (1997) 2943.